The role of liquid viscosity and of air entrapped on the splashing of drops impacting over superhydrophobic substrates

Paula García-Geijo, Guillaume Riboux, and José Manuel Gordillo*
Área de Mecánica de Fluidos, Departamento de Ingeniería Aeroespacial y Mecánica de Fluidos, Universidad de Sevilla, Avenida de los Descubrimientos s/n 41092, Sevilla, Spain.
(Dated: September 8, 2022)

Here we analyze the splash transition of drops of liquids with different viscosities impacting normally over different types of rough superhydrophobic substrates, finding that the velocity for the splash transition, V^*, increases for increasing values of the liquid viscosity and also when the proportion of air entrapped at the substrate corrugations decreases. Our experimental results also reveal that the amount of air entrapped between the substrate and the wall increases with the value of the relative roughness $\epsilon = \varepsilon/R$, with ε and R indicating the amplitude of the corrugations and the radius of the drop, respectively. We show that our experimental values of V^*, as well as those reported in similar contributions in the literature, can be predicted using the splashing model presented in [Quintero, Riboux, and Gordillo, Splashing of droplets impacting superhydrophobic substrates, Journal of Fluid Mechanics 870, 175 (2019)], once the liquid shear stress at the wall is expressed as a decreasing function of ϵ namely, of the proportion of air entrapped at the substrate.

INTRODUCTION

Superhydrophobic surfaces are characterized by a large value of the apparent contact angle, by a low value of the contact line hysteresis and also by the fact that the interfacial protrusions induce the piercing of the thin liquid sheet which is created after a drop impacts the substrate [2, 3]. The combination of all these effects contribute to reduce the contact time of the liquid with the solid and to reduce friction, increasing the fluid velocity along the substrate, hence favoring the self-cleaning of the interface and its ability to stay dry and thermally insulated [2–4]. In fact, it is well accepted that the superhydrophobic behaviour of natural or engineered substrates is caused by tiny asperities at the surfaces of solids where air is entrapped, increasing the value of the apparent contact angle. Indeed, [5] expressed the value of the apparent contact angle θ on a corrugated substrate as a function of θ_0 namely, the Young or chemical contact angle corresponding to a flat surface made of the same material, finding that $\theta > \theta_0$ if $\theta_0 > \pi/2$ [6–10].

It is well known that the interesting properties of superrepelent surfaces described above are used in natural world, where the leaves of many types of plants and also the wings and legs of different animals are decorated with micron-sized bumps with superimposed fine nanostructures made of a hydrophobic material [4, 10, 11]. These hierarchical structures are believed to confer robustness to the superhydrophobic behaviour of surfaces and, in fact, it will be shown next that the air pockets entrapped in the corrugations created by the type of artificial coating used in the present experimental study are stably mantained between the interstices even when a drop impacts the solid.

We have mentioned above that one of the key features and main advantages of using superhydrophobic coatings is their ability to reduce both the contact area and the contact time between the solid and the liquid when a drop impacts the substrate. The solid-liquid interaction is reduced even further when the drop splashes namely, when the drop disintegrates into small pieces which are rapidly ejected outwards after contacting the solid. Precisely, the main objective of our study is to determine if a drop impacting a superrepelent substrate will splash or not. For this purpose, in this contribution we will quantify the splash threshold conditions as a function of the substrate roughness and of the liquid material properties.

It has been recently shown that the value of the critical velocity for splashing at normal atmospheric conditions decreases for increasing values of the apparent contact angle -see e.g., [1, 12, 13]. This observation can be explained by the fact that splashing occurs due to the growth of capillary disturbances developing at the rim bordering the liquid sheet that expands radially outwards once the drop touches the wall. For the case of partially wetting substrates, the growth of the capillary disturbances is inhibited when the rim is in contact with the solid and, therefore, the splashing velocity is fixed by the condition that the rim needs to be separated from the wall first [14], a process which is favoured when the advancing contact angle increases in the case the liquid partially wets the substrate [15]. However, for the case of superhydrophobic coatings, the advancing rim is not in contact with the substrate even for impact velocities smaller than the splash threshold (see Fig. 1) and, hence, capillary instabilities can develop easier, this being the reason for the smaller critical velocity for splashing observed in experiments done using superrepelent surfaces. This is also the reason for the differences between the splash criterion presented in [1], applicable for the case of superhydrophobic substrates and, consequently, when the rim does not touch the substrate, and that in [14], deduced for the case of partially wetting substrates.

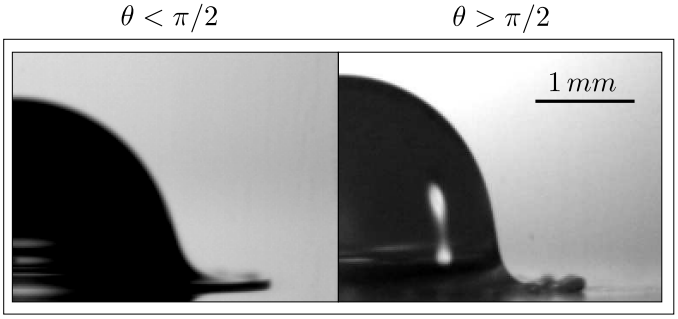

FIG. 1. Impact with a velocity of $V = 2.22 \pm 0.02$ ms^{-1} of a water drop of radius $R = 1.43 \pm 0.03$ mm over a smooth glass substrate (left: the value of the static contact angle θ is $\theta < \pi/2$ and, therefore, the liquid partially wets the substrate) or over a smooth Teflon substrate (right: $\theta > \pi/2$, hydrophobic substrate).

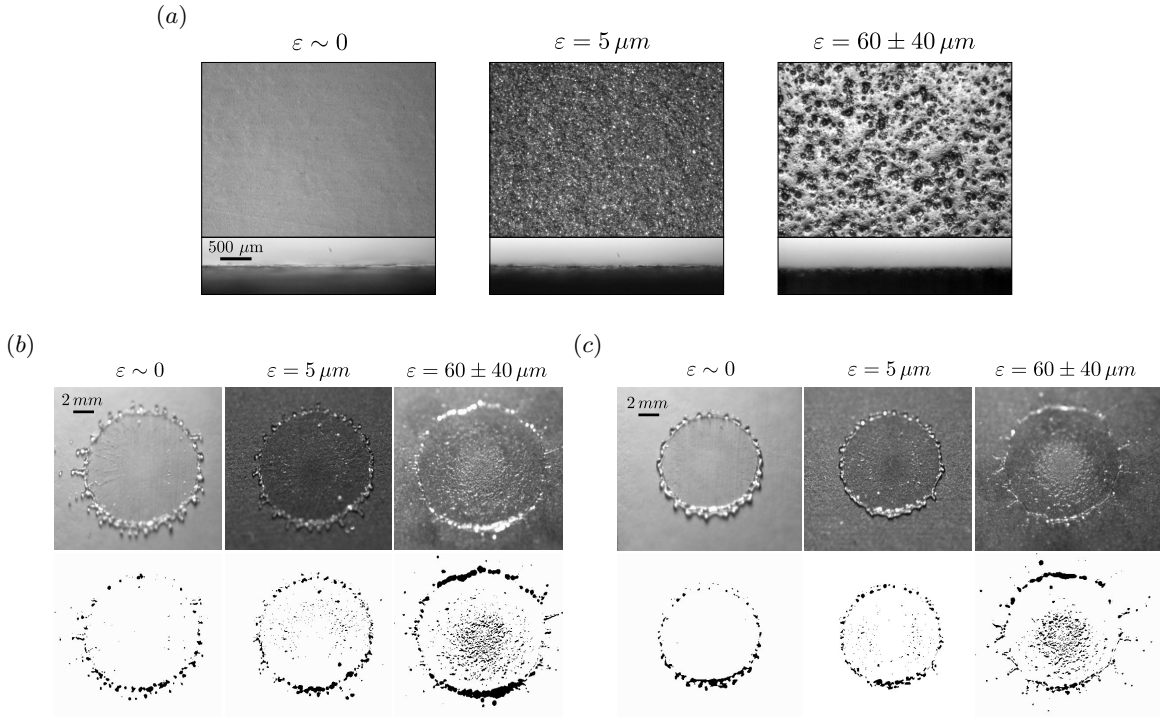

FIG. 2. (a) Front and lateral view of different superhydrophobic substrates of increasing roughnesses. (b) The images show the impact with a velocity of $V = 2.95 \pm 0.01$ ms^{-1} of water drops of radius $R = 1.47 \pm 0.02$ mm over the three types of substrates depicted in (a) at $t = TV/R = 4 \pm 0.03$, with the value of the substrate roughness ε increasing from left to right. (c) The images show the impact with a velocity $V = 2.85 \pm 0.02$ ms^{-1} of drops of radius $R = 1.42$ mm of a 30% water-sugar mixture with a viscosity of three times that of water over the three substrates in (a) at $t = TV/R = 4 \pm 0.03$ with the value of the substrate roughness increasing from left to right. The images in (b) and (c) illustrate that the proportion of air bubbles entrapped between the solid and the expanding lamella increases with the value of ε. The presence of air bubbles can be more clearly appreciated from the processed images at the bottom of (b) and (c), where gas regions are visualized in black. Here, T indicates the instant of time after the drop first touches the substrate.

Our study is motivated by the experimental results in [1, 12, 13, 15–23], which show that large values of the apparent contact angle θ favor the splash transition and also by those in [24–26], which suggest that the critical velocity for splashing decreases for increasing values of the amplitude ε of the asperities of roughened superhydrophobic substrates. The results presented here can also be extended to the case in which the drop impacts a superheated wall in the so-called dynamic Leidenfrost regime [27–29], which is characterized by the fact that a thin vapour layer prevents the contact between the liquid and the solid.

Then, the main objective in this contribution is to analyze the impact of millimetric drops of liquids with different viscosities over hydrophobic substrates of varying random roughnesses and we will mainly focus on the characterization

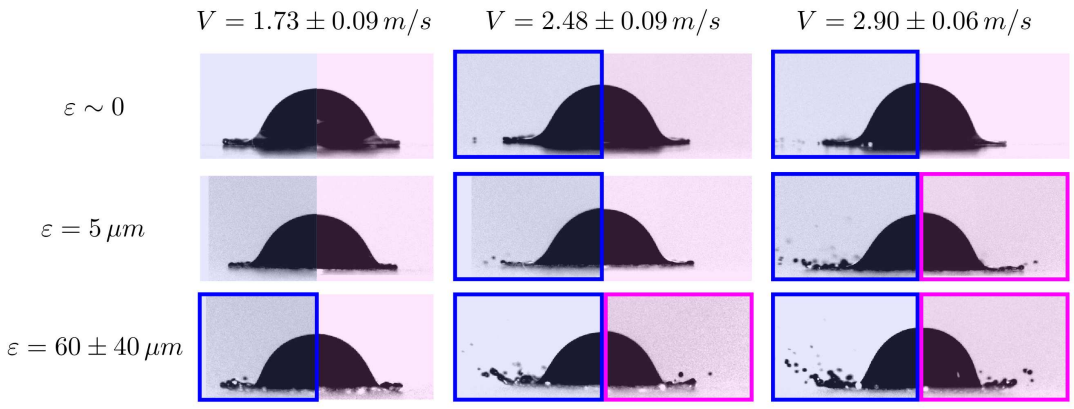

FIG. 3. Images showing the impact with different velocities of drops of radius $R = 1.44 \pm 0.05$ mm of either water (blue background) or of a 30% water-sugar mixture with a viscosity of three times that of water (pink background) over three different types of superhydrophobic substrates with increasing roughnesses. The blue or pink boxes are used to highlight the occurrence of splashing. The value of the advancing contact angle is the same, $\theta_{adv} \approx 158^{\circ}$, for the cases of Teflon $\varepsilon \approx 0$ μm, and for the case of glass covered with three layers of Neverwet, $\varepsilon = 60 \pm 40$ μm, see table II. The images are represented at $t = T\,V/R = 0.8 \pm 0.08$, with T the instant of time after the drop first touches the substrate.

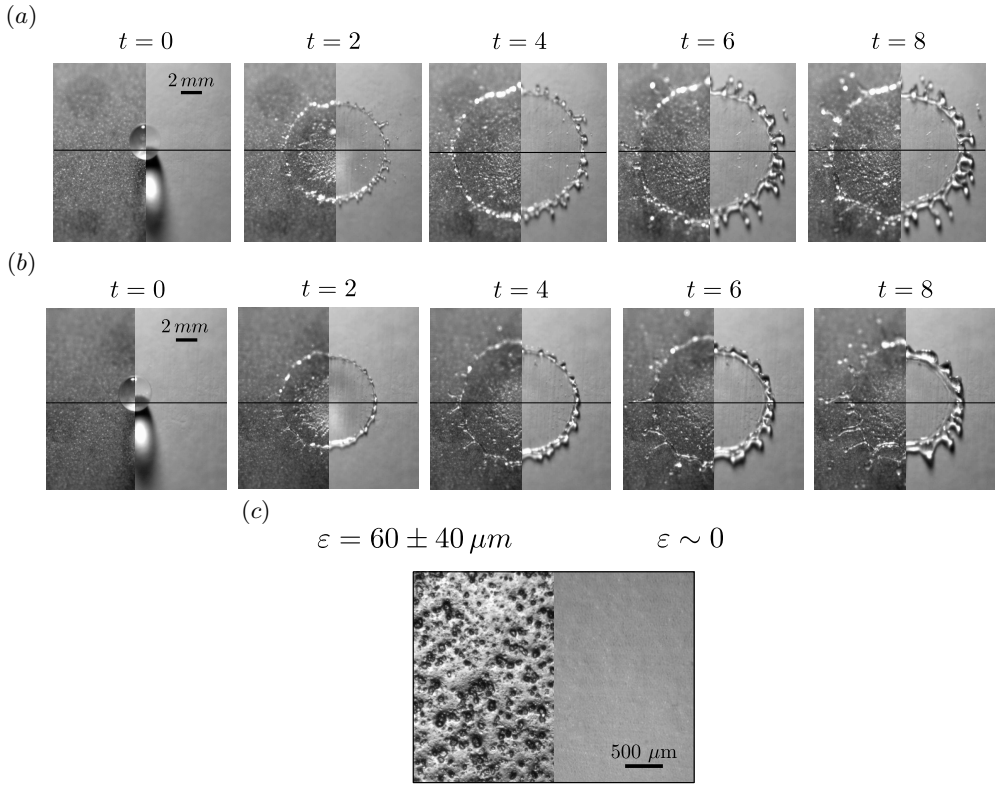

FIG. 4. Spreading of a drop of radius $R = 1.45 \pm 0.03$ mm of either water (a) or a 30% sugar-water mixture (b) impacting with a velocity $V = 2.89 \pm 0.05$ ms^{-1} over two different types of superhydrophobic substrates with different rugosities. (c) At the left of each of the images in (a) and (b), drops impact against glass coated with several layers of Neverwet, ($\varepsilon = 60 \pm 40$ μm) and, at the right, drops impact over PTFE (Teflon, $\varepsilon \approx 0$ μm). For both values of the liquid viscosity, the maximum expansion of the drop is attained for the case of the superhydrophobic substrate with the larger value of ε (left images). Here, $t = TV/R$, with T the instant of time after the drop first touches the substrate.

of the critical conditions under which the splash transition at normal atmospheric conditions takes place namely, the minimum value of the impact velocity for which the rim bordering the expanding liquid sheet ejected after impact breaks into tiny droplets. The analogous case of drop splashing at rough partially wetting substrates is considered at length in [15, 23] and references therein.

With this purpose in mind, we have carried out a series of experiments in which drops of liquids of varying viscosities are impacted against superhydrophobic substrates with different rugosities, see Fig. 2a. Our experiments in Figs. 2b-c reveal that the amount of air entrapped at the substrate corrugations increases with the value of the relative roughness, $\epsilon = \varepsilon/R$, with ε and R respectively indicating the amplitude of the corrugations and the radius of the drop. One of the consequences of increasing the amount of air entrapped at the substrates depicted in Figs. 2b-c is illustrated in Fig. 3: the critical velocity for splashing, V^*, decreases for increasing values of ϵ namely, when the proportion of air entrapped at the substrate increases. Moreover, the experimental results depicted in Fig. 3 indicate that the critical velocity for splashing increases with the liquid viscosity. Notice also that Figs. 2 and 3 also reveal that the different values of the splash velocity are not associated with the advancing contact angle, θ_{adv}, which is identical for the case of Teflon ($\epsilon \approx 0$) and the superhydrophobic substrate with the largest value of ϵ: in fact, Figs. 2 and 3 indicate that V^* is larger for the case of the smoother surface, which is the one for which less air is entrapped between the liquid and the wall. In addition, Fig. 4 reveals that the value of the maximum radial extension of drops impacting over Teflon is smaller than for the case the drop impacts the roughest superhydrophobic substrate. All these experimental evidences suggest that the main effect of ε on the splash transition of drops impacting superhydrophobic substrates is to increase the amount of air entrapped at the substrate corrugations. This effect reduces the liquid shear stresses at the wall and, hence, increases the fluxes of mass and momentum into the rim bordering the expanding liquid sheet. Using the model in [1], here we will show that the larger fluxes of mass and momentum into the rim favor the growth of capillary instabilities, this being the reason behind the experimental observations in Fig. 3 indicating that the splash velocity decreases when the proportion of gas entrapped between the liquid and the wall increases or when the liquid viscosity decreases.

EXPERIMENTAL SET-UP AND PHENOMENOLOGY

Experiments are carried out letting drops of radii R of different water-sugar mixtures with density ρ, viscosity μ and interfacial tension coefficient σ -see table I- fall at normal atmospheric conditions in a gaseous environment of viscosity μ_g over superhydrophobic surfaces of different roughnesses and with different values of the apparent contact angle, see table II. The impact velocity V is changed by controlling the height from which drops impact the different types of substrates and experiments are repeated once the previous sample is replaced by a clean one. The main purpose of this experimental study is to determine, for each type of substrate and for each type of liquid, the so-called splash threshold velocity, V^*, which is defined here as the minimum value of the impact velocity V for which the drop splashes namely, disintegrates into tiny pieces rapidly ejected radially outwards. The impact process is recorded using two high-speed cameras: a Phantom V7.3 for the lateral views, from which the radii and velocities of the falling drops are measured, and a Phantom V710 forming an angle of 30° with the vertical direction for the top views. Experiments are illuminated using two light sources with their corresponding diffusers, the lateral/top cameras are respectively operated at 13029/40989 f.p.s. (frames per second) and the spatial resolution of the images acquired is 20/46 microns per pixel.

In the following, the results of the analysis will be presented in terms of the following dimensionless parameters:

$$We = \frac{\rho V^2 R}{\sigma}\,, \quad Oh = \frac{\mu}{\sqrt{\rho R \sigma}}\,, \quad Re = \frac{\sqrt{We}}{Oh}\,, \quad \epsilon = \frac{\varepsilon}{R} \quad \text{and} \quad \theta\,, \tag{1}$$

namely, the Weber, Ohnesorge, Reynolds, the relative roughness of the substrate and the apparent static contact angle, defined using R, R/V and ρV^2 as the characteristic scales of length, time and pressure.

The values of the apparent static contact angle, θ, are always larger than $\pi/2$ rad and the relative roughnesses of the different types of substrates used is such that $\epsilon \lesssim 0.1$ i.e., the amplitude of the surface corrugations is much smaller than the drop radius, see table II. The smallest value of ϵ corresponds to a smooth teflon substrate (PTFE), for which the amount of air entrapped is minimum and, therefore, the value of the friction with the wall is expected to be the largest. The rest of surfaces investigated possess much larger values of ϵ and, hence, the amount of air entrapped is larger and, hence, the friction with the wall is expected to be smaller than for the case of PTFE. Table II shows that, as it was done in [15], we have also made use of silicon-carbide (SC) sandpapers and of aluminium-oxide (AO) lapping films with different grit sizes. In addition, we have also considered different types of superhydrophobic substrates

TABLE I. Physical properties of the three different water/sugar mixtures used in experiments. The values of the density and viscosity have been extracted from *lclane.net/text/sucrose.html*. The surface tension data correspond to our own measurements, conducted making use of the pendant drop method and have been analyzed using the software 'Attension Theta'. Notice that surface tension value increases with the sugar content since the ionic strength of the solution increases with the amount of sugar added.

Liquid	$\rho\ (kg/m^3)$	$\mu\ (mPa \cdot s)$	$\sigma\ (mN/m)$	$R\ (mm)$	Oh
WS00%	1000	1.0	72.2 ± 0.1	1.46	0.0031
WS10%	1038	1.3	73.0 ± 0.2	1.45	0.0040
WS30%	1127	3.2	73.9 ± 0.1	1.42	0.0091

TABLE II. The table reflects the range of Weber numbers covered for each of the different liquids -see table I- and substrates used in the experimental study: SH0, SH1 and SH2 refer to glass slides coated with different number of layers of *Neverwet* (SH0 three layers, SH1 two layers and SH2 one layer) and the corresponding values of the roughness ε, which increases with the number of layers [3, 20]. We have not measured the values of ε for these substrates and the values shown in the table are taken from [3, 20]; SC P4000, SC P6000 and AO 'White' refer to different types of sandpapers using the manufacturer's terminology, with their roughnesses provided by the manufacturer -see [15] for details- and $\varepsilon \simeq 0$ for the case of Teflon substrates (PTFE). The values of the static, advancing and receding contact angles indicated in the table for each type of liquid and each type of substrate correspond to our own experimental measurements, which contain errors of $\pm 10^\circ$, this being the reason why the value of the static contact angle is, in some cases, larger than the corresponding value of the advancing contact angle.

Liquid	Surf.	$\varepsilon\ (\mu m)$	We	θ	θ_{adv}	θ_{rec}
WS00%	SH0	60 ± 40	$45 - 181$	157°	159°	156°
	SH1	60 ± 40	$45 - 182$	124°	154°	86°
	SH2	60 ± 40	$57 - 181$	90°	105°	47°
	SC P4000	5	$56 - 221$	117°	136°	71°
	SC P6000	4	$89 - 161$	112°	110°	38°
	AO White	0.3	$62 - 230$	100°	102°	76°
	PTFE	~ 0	$55 - 199$	136°	158°	97°
WS10%	SH0	60 ± 40	$46 - 190$	158°	162°	150°
	SH1	60 ± 40	$46 - 190$	126°	153°	84°
	SH2	60 ± 40	$58 - 190$	88°	104°	45°
	SC P4000	5	$56 - 227$	117°	136°	71°
	SC P6000	4	$90 - 163$	116°	130°	52°
	PTFE	~ 0	$58 - 202$	137°	154°	106°
WS30%	SH0	60 ± 40	$62 - 207$	150°	157°	145°
	SH1	60 ± 40	$64 - 209$	115°	146°	55°
	SH2	60 ± 40	$64 - 206$	90°	96°	44°
	SC P4000	5	$60 - 239$	110°	136°	51°
	SC P6000	4	$130 - 209$	118°	108°	34°
	AO White	0.3	$195 - 239$	110°	97°	10°
	PTFE	~ 0	$63 - 253$	132°	157°	84°

created by depositing one (SH2), two (SH1) or three (SH0) layers of *NeverWet*: the larger the number of layers of Neverwet, the larger is the surface roughness, which varies within the range $\varepsilon = 60 \pm 40$ μm, see table II [3, 20]. The liquid viscosity has been varied by considering water/sugar mixtures with different proportions in weight of sugar. The sugar concentration is low enough for non-newtonian effects to be absent [30], see tables I and II, where it can be also observed that the values of the apparent contact angles do not depend significantly on the sugar concentration.

The superhydrophobic-like behaviour of all the surfaces and liquid viscosities considered in this study can be further appreciated in Fig. 5, where it is observed that the rim retracts once the maximum expansion of the impacting drops is reached. Notice also in Fig. 5 that the bright area in the images corresponding to the SH0 substrate, which is the signature of the presence of bubbles, is more clearly visible than in the case of the other two substrates in the figure.

Figure 6 summarizes the main experimental results obtained in this study since it provides the values of the critical Weber numbers characterizing the splash transition for the different liquids and the different types of substrates considered here. Notice that the general trend is that the critical Weber number for splashing, defined as the minimum value of the Weber number for which drops are ejected from the rim, increases when the liquid viscosity is

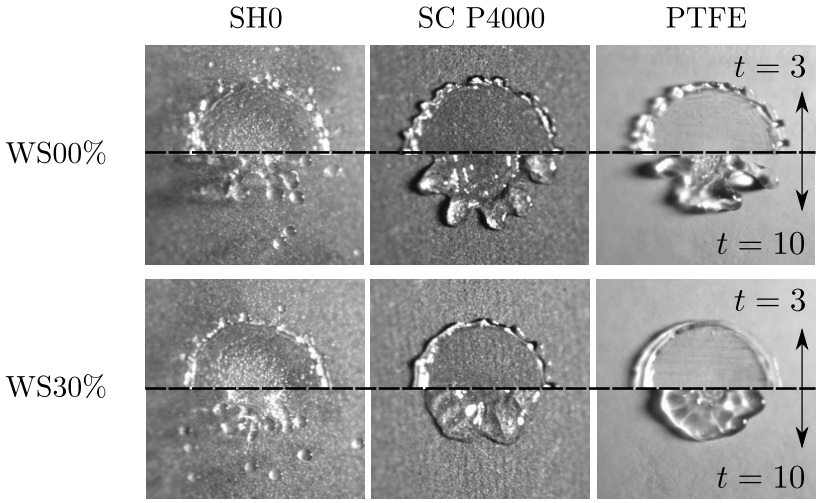

FIG. 5. The images show the impact of drops over three of the different types of substrates investigated in this study at two different instants of time, $t = TV/R = 3 \pm 0.03$ (top part of each image) and $t = 10 \pm 0.2$ (bottom part of each image), with T the instant of time after the drop first touches the substrate, for a nearly constant value of the Weber number $We = 77 \pm 10$ and two values of the Ohnesorge number: $Oh = 3.1 \times 10^{-3}$ for the case of water drops -images at the top- and $Oh = 9.1 \times 10^{-3}$ for the case of the 30% water-sugar mixture. As it is expected for the case of superhydrophobic substrates, the rim retracts after reaching the maximum expansion. Notice also that the bright area in each of the images, which is the signature of the air entrapped in the corrugations, is much larger for the case of the SH0 substrate, which is the one with the largest value of ε -see table II.

TABLE III. Experimental values of the critical Weber number, We^*, for each of the liquids and each of the substrates used in the present study, see Fig. 10 and table I.

Liquid	Symbol	ε (μm)	We^*	Surface Name
			56.6	SH0
	♦	60±40[a]	62.2	SH1
			67.3	SH2
WS00%	●	5	107.1	SC P4000
	▲	4	130.9	SC P6000
	▼	0.3	130.7	AO White
	■	∼0	112.4	PTFE
			69.2	SH0
	◊	60±40[a]	69.3	SH1
WS10%			94.3	SH2
	○	5	112.3	SC P4000
	△	4	144.7	SC P6000
	□	∼0	117.8	PTFE
			86.1	SH0
	♦	60±40[a]	99.5	SH1
			111.5	SH2
WS30%	●	5	156.1	SC P4000
	▲	4	165.1	SC P6000
	▼	0.3	220.6	AO White
	■	∼0	196.9	PTFE

[a] Based on the values reported by [3, 20].

increased or when the amplitude of the corrugations decreases namely, when the proportion of air entrapped at the substrate decreases, see Fig. 2.

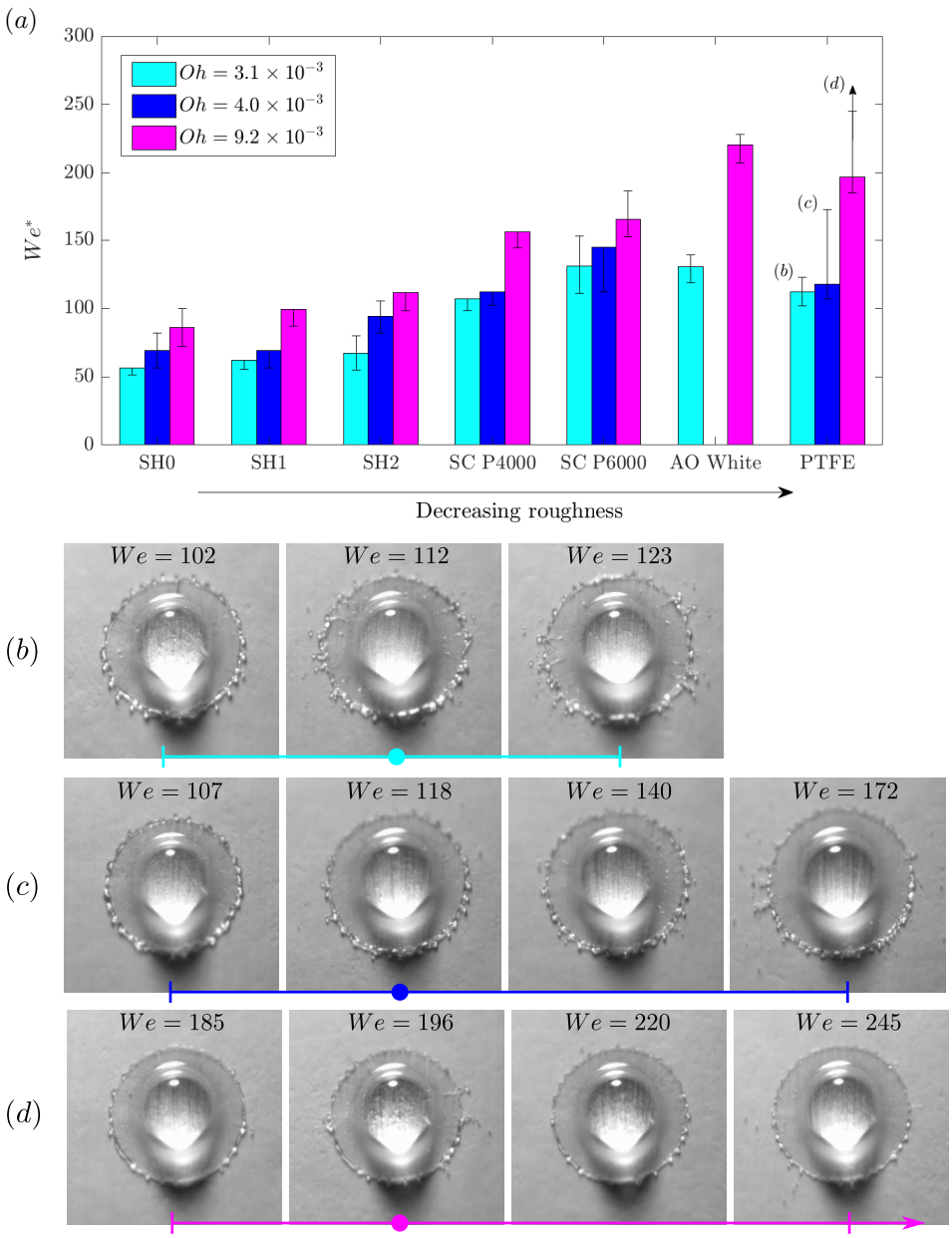

FIG. 6. The experimental values of the critical Weber number for splashing, We^*, are represented for three values of the Ohnesorge number and decreasing values of the substrate roughness, see table III. The general trend is that We^* increases if Oh increases or ε decreases. Since the value of We^* is unclear in some cases, we include in (a) error bars and in (b)-(d) we show experiments carried out using the PTFE substrate revealing that, in this case, the number of droplets ejected increases very smoothly with We, this fact justifying the error bars in (a).

MODELING AND COMPARISON WITH EXPERIMENTS

In this section we provide details of the model developed in [1] to describe the splash transition of drops impacting superrepelent surfaces of interest here, $\theta > \pi/2$. In the following, dimensionless quantities, defined using R, R/V and ρV^2 as characteristic values of length, time and pressure, are written using lower case letters to differentiate them from their dimensional counterparts, in capitals.

The splash criterion in [1], applicable for the case of superhydrophobic substrates, notably differs from the splash criterion presented in [14]. Indeed, for the case of hydrophobic solids, the advancing rim is already separated from the substrate even for impact velocities below the splash threshold (see Fig. 1) and, therefore, drop splashing is limited

TABLE IV. Experimental values of the critical Weber number We^* reported by [19, 20, 24, 25, 29, 31–33], see Fig. 10, corresponding to different values of Oh and different types of superhydrophobic substrates. LF is used to denote experiments of drops impacting in the Leidenfrost regime and χ indicates the inclination angle with the horizontal.

Ref.	Symbol	R (mm)	ε (μm)	Oh	We^*	Surface
Gupta, Vaikuntanathan & Sivakumar (2016) [20]	●	1.50	50±20[a]	0.0027	57.9	Al + *NeverWet*
Hamlett *et al.* (2013) [31]	●	1.01[b]	32–45	0.0037	55.0	Glass covered with hydrophobic spheres
			63–75		41.7	
			75–80		39.0	
			80–90		38.7	
			90–106		47.4	
			125–140		38.1	
			180–212		58.4	
Kim *et al.* (2014) [25]	●	0.88[b]	15.8[c]	0.0040	93.1	G20
			20.3[c]		87.6	G30
			19.9[c]		77.0	G40
			12.2[c]		77.9	G50
Kim *et al.* (2012) [24]	●	0.66	25.8[d]	0.0046	57.3	Micro-nano surface
Chen *et al.* (2011) [19]	●	1.38	10[e]	0.0028	40.8	Lotus leaf
	●		21.3[d]		74.2	NG surface
	○		> 20[f]		40.8	Lotus leaf modified
Staat *et al.* (2015) [32]	▶	1.25	–	0.0075	77.5	LF
Wang *et al.* (2020) [29]	▶	1.05	–	0.0073		Inclined LF
					63.7	$\chi = 0°$
					67.7	$\chi = 15°$
					66.4	$\chi = 30°$
					70.9	$\chi = 45°$
					66.0	$\chi = 60°$
Liu, Cai & Tsai (2020) [33]	▶	1.18	–	0.0034	42.8	Smooth LF

[a] Based on the reported profilometer measurements along the substrate.
[b] Oh is computed using the mean radius of the different sizes reported.
[c] ε is calculated through the reported value of R_a using the empirical equation given in [15], $R_a = 0.943 + 0.134\varepsilon$ with all quantities in microns.
[d] The value of ε is not provided in the reference and it is approximated here as the equivalent diameter of a sphere with the same volume as that of the pillars.
[e] The value of ε is not provided in the reference and it is approximated here as the diameter of the irregularly distributed microbumps depicted over the SEM lotus leaf images.
[f] The value of ε is assumed to be twice the value in [e]

in the case of interest here by the ability of the rim to break into droplets, not by the condition that the rim needs to be first separated from the substrate, as it is the case of partially wetting solids [14]. As it was discussed in [35], the edge bordering the expanding lamella of thickness $B = Rb$ disintegrates into tiny droplets as a consequence of the amplifications of capillary disturbances with a characteristic wavelength $\Lambda \simeq \pi B/0.7$ for which Rayleigh's classical stability analysis [36] predicts the fastest growth rate of capillary perturbations developing in a liquid cylinder of diameter B. The growth of the most unstable capillary instabilities break a liquid cylinder into drops in characteristic time of $3T_c$ [37] with $T_c = (\rho B^3/8\sigma)^{1/2}$ the capillary time. However, for the case of interest here, the growth of capillary instabilities is highly attenuated as a consequence of the simultaneous growth of the rim diameter. Indeed, for a fixed value of $\Lambda \simeq \pi B/0.7$, the initial value of the ratio $\Lambda/B = \pi/0.7$ decreases during the time of growth of capillary disturbances, $3T_c$, to a value $\Lambda/[(B + \Delta B)]$ with $\Delta B = 3\,T_c \times dB/dT$. Therefore, since capillary disturbances can disintegrate the rim only if $\Lambda/[(B + \Delta B)] > \pi$ -this is so because of the fact that disturbances of wavelength $\Lambda \leq \pi B$ are linearly stable [36]- and taking into account that $\Lambda \simeq \pi B/0.7$, the critical condition for splashing in superhydrophobic substrates can be expressed as [35]:

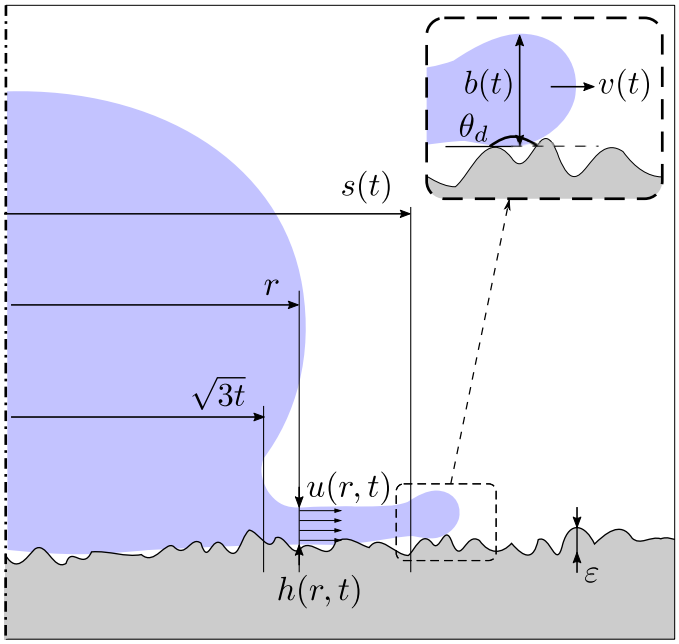

FIG. 7. Sketch illustrating the definitions of the different dimensionless variables used in the model, $s(t)$, $v(t)$, $b(t)$, $u(r,t)$ and $h(r,t)$ [34], which are defined using as characteristic values of length, time and pressure, R, R/V and ρV^2, with R, V and ρ denoting, respectively, the drop radius, the impact velocity and the liquid density. The value for the dynamic advancing contact angle is taken here as $\theta_d = \pi$.

$$\frac{B}{B+\Delta B} > 0.7 \Rightarrow 1 + 3\,T_c \frac{1}{B}\frac{d\,B}{d\,T} < 0.7^{-1} \Rightarrow C_b = \sqrt{\frac{b}{8}}\,\frac{\mathrm{d}b}{\mathrm{d}t}\,We^{1/2} \lesssim 0.1\,. \tag{2}$$

Using the results in [1, 34], both the rim thickness $b(t)$ and also db/dt in Eq. (2) are calculated solving the mass and momentum balances at the rim, located at $r = s(t)$, see Fig. 7:

$$\begin{cases} \dfrac{\pi}{4}\dfrac{db^2}{dt} = [u(s,t) - v]\,h(s,t)\,, \qquad \dfrac{ds}{dt} = v\,, \\ \dfrac{\pi b^2}{4}\dfrac{dv}{dt} = [u(s,t) - v]^2\,h(s,t) - 2We^{-1}\,. \end{cases} \tag{3}$$

Notice that the last term in the last of the equations in (3) should be written as $-(1+\beta)\,We^{-1}$ with $\beta = -\cos\theta_d$, with θ_d the value of the dynamic advancing contact angle, see figure 7. Since the apparent contact angle for rough substrates is $\theta > \theta_0 > \pi/2$ [5] and because of the fact that the dynamic contact angle is $\theta_d > \theta$ because θ_d increases with the capillary number based on the velocity of the rim velocity, here we have taken $\theta_d \approx \pi$ and, hence, $\beta = 1$, which has been proven to be an excellent approximation in the description of the spreading of of drops impacting against solid substrates [34, 38]. Different cases with $\beta < 1$ are considered in the Appendix.

Equations (3) are solved particularizing at $r = s(t)$ the expressions for the velocity $u(r,t)$ and the thickness of the lamella $h(r,t)$, see Fig. 7, given by:

$$\begin{cases} u(r,t) = \dfrac{r}{t} - \dfrac{Re^{-1/2}}{t}\left[\dfrac{\sqrt{3}\,\chi\,x}{2\,h_a(x)} + \dfrac{2\sqrt{3}\lambda}{7h_a(x)x^{5/2}}\left(t^{7/2} - x^{7/2}\right)\right] + O(Re^{-1})\,, \\ h(r,t) = 9\dfrac{t^2}{r^4}h_a(x) + \dfrac{Re^{-1/2}}{rt}\left[\dfrac{\sqrt{3}}{2}x^2 + \dfrac{\sqrt{3}(105\,\chi - 60\lambda)}{42}x^3\left(t^{-1} - x^{-1}\right) + \dfrac{24\sqrt{3}\lambda}{105}x^{-1/2}\left(t^{5/2} - x^{5/2}\right)\right] + O(Re^{-1})\,, \end{cases} \tag{4}$$

deduced in [34] assuming that the velocity varies linearly with the normal distance to the wall within the boundary layer of thickness $\propto \sqrt{t/Re}$ [39], taking into account that the velocity profiles are uniform when the normal distance to the wall is larger than the width of the boundary layer and applying integral balances of mass and momentum at

a differential portion of the lamella. In Eq. 4, $x = 3\,(t/r)^2$, $\chi = 0.6$, $h_a(x)$ refers to the thickness of the lamella in the potential flow limit $Re \to \infty$ calculated using the polynomial approximation provided in [34] and λ is the friction factor, which was set to $\lambda = 1$ in [34] and it is related with the dimensionless shear stress at the substrate τ_w as

$$\tau_w = \lambda \frac{u}{\sqrt{Re\, t}}\,, \tag{5}$$

with this expression implicitly assuming that the no-slip boundary condition is satisfied at the wall when $\lambda = 1$. In the present case, however, the shear stress balance at the air-liquid interface reveals that $\lambda \approx 0$ at the regions occupied by the gas. Indeed, notice that the thickness of the air layer where gas pockets are entrapped is $\sim \varepsilon$ and the thickness of the liquid boundary layer is $\propto R\sqrt{t/Re}$ [39]. Then, since the maximum value of the gas shear stress can be estimated assuming that velocity at the gas-liquid interface is Vu, the value of λ in the region occupied by the gas can be estimated from the shear stress balance

$$\rho\, V^2\, \tau_w \lesssim \mu_g \frac{Vu}{\varepsilon} \Rightarrow \lambda \lesssim \frac{\mu_g}{\mu} \epsilon^{-1} \sqrt{\frac{t}{Re}}\,, \tag{6}$$

where we have made use of equation (5). Then, since $\mu_g/\mu \sim 10^{-2}$, $Re \sim 10^3$ and $t \lesssim 1$, the balance in equation (6) reveals that $\lambda \ll 1$ whenever $\epsilon \gtrsim 10^{-3}$ namely, whenever the thickness of the gas layer is larger than $10^{-3}\, R \sim 10^{-6}$ m, where in this latter estimation we have considered the case of millimetric drops, $R \sim 10^{-3}$ m. The values in table II reveal that, indeed, $\varepsilon \gtrsim 1\ \mu m$ and, moreover, the experimental results in [40] reveal that the thickness of the vapor layer beneath a drop impacting a superheated substrate in the Leidenfrost regime is also $\gtrsim 1\ \mu m$. Then, in the Leidenfrost regime, $\lambda \approx 0$ because, in this case, a continuous vapor layer prevents the contact between the solid and the liquid all along the radial extension of the impacting drop. However, for the case of superhydrophobic substrates, the shear stress changes from zero at the discrete regions occupied by the gas -these regions possess a characteristic lateral width given by the size of the asperity $\sim \varepsilon$, to $\lambda \sim 1$ along the regions where the liquid contacts the wall, also of characteristic width $\sim \varepsilon$. Therefore, for the case of superhydrophobic substrates, the liquid sheet, which extends radially outwards a characteristic distance $\sim R$, will be alternatively in contact with the wall and with the gas-liquid interface along regions of width $\sim \varepsilon$. Consequently, for the case of superhydrophobic substrates, the shear stress at the wall in equation (5) can be viewed as an averaged value which is calculated along a length $\varepsilon \ll \ell \ll R$ that includes regions where the liquid contacts the wall ($\lambda \sim 1$) and others where the gas pockets are entrapped ($\lambda \approx 0$ if $\epsilon \gtrsim 10^{-3}$). It is not the purpose here to develop a self-consistent theory expressing the dependence of the dimensionless friction factor λ as a function of the relative roughness, $\epsilon = \varepsilon/R$. Instead, here we propose an empirical model for $\lambda(\epsilon)$ which takes into account the facts that: if $\epsilon \lesssim 10^{-3}$ namely, if the liquid contacts the wall all along the radial extension of the liquid sheet or the thickness of the gas layer is so thin so as to approximately enforce the no slip consition -see equation (6)- $\lambda = 1$ but, if the width of the regions occupied by the gas pockets relative to the radial extension of the liquid sheet is above a certain threshold, the shear stress will decrease down to zero.

In other words, for the case of droplets in the dynamic Leidenfrost regime in which the solid-liquid contact is lubricated by a continuous vapor layer, $\tau_w \simeq 0 \Rightarrow \lambda = 0$ [28], and in those cases in which the proportion of gas pockets tends to zero, the shear stress at the wall is given by equation (5) with $\lambda = 1$. The experimental observations depicted in Fig. 2, which reveal that the proportion of air entrapped at the substrate corrugations increases with ε, indicate that the cases considered in this contribution are in between these two extreme limits. Hence, in order to quantify the shear stress at the wall, which influences the time evolution of $b(t)$ through the mass and momentum fluxes into the rim as it is expressed by Eqs. (3)-(4), here we propose to evaluate the shear stress at the wall using equation (5) but modifying the expression of λ in such a way that, if no air bubbles were entrapped $\lambda(\epsilon \ll 1) = 1$ but, if the liquid-solid contact is prevented by a continuous gas layer, as it is the case of drops in the dynamic Leidenfrost regime, $\lambda = 0$. Then, the unknown equation for λ should recover the no slip limit in [34] namely, $\lambda(\epsilon = 0) = 1$, should also reflect the fact depicted in Fig. 2 that the proportion of air entrapped increases with $\epsilon = \varepsilon/R$ when $\epsilon \approx 0$, and hence, $d\lambda/d\epsilon(\epsilon \approx 0) < 0$, and should also recover the Leidenfrost limit $\lambda = 0$ when the proportion of air entrapped at the substrate corrugations is sufficiently large. Here we propose following empirical piecewise linear equation for $\lambda(\epsilon)$, which is the simplest possible relationship satisfying the previous restrictions:

$$\lambda = 1 - \epsilon/\epsilon_0 \quad \text{if} \quad \epsilon \leq \epsilon_0 \quad \text{and} \quad \lambda = 0 \quad \text{if} \quad \epsilon > \epsilon_0\,, \tag{7}$$

where only the free parameter ϵ_0 needs to be adjusted to the experimental data.

The system of ordinary differential equations (3)-(4) is integrated from $t = t_e$, with $t = t_e$ the ejection time of the lamella sketched in Fig. 7a, calculated using the equation deduced in [14], which retains the effect of the liquid boundary layer in the process of ejection of the liquid sheet

$$\sqrt{3}/2\, Re^{-1}\, t_e^{-1/2} + Re^{-2} Oh^{-2} = 1.1^2\, t_e^{3/2} \tag{8}$$

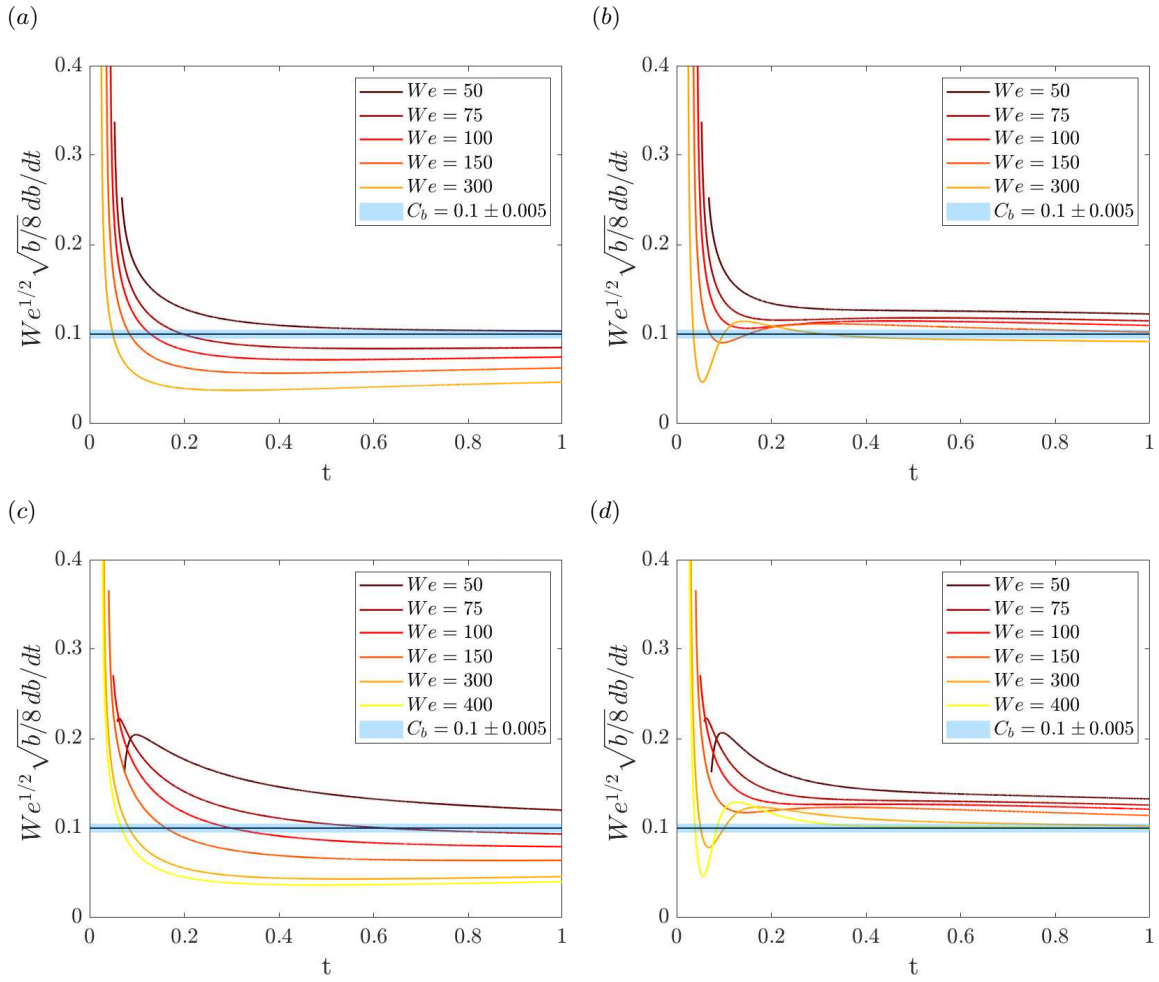

FIG. 8. The ratio $C_b = We^{1/2}\sqrt{b/8}\,db/dt$ defined in Eq. (2) is calculated solving the system of Eqs. (3)-(4) subjected to the initial conditions given in Eqs. (8) and (10) for different values of We and two values of λ and Oh: (*a*) $Oh = 3 \times 10^{-3}$ and $\lambda = 0$, (*b*) $Oh = 3 \times 10^{-3}$ and $\lambda = 1$, (*c*) $Oh = 9 \times 10^{-3}$ and $\lambda = 0$ and (*d*) $Oh = 9 \times 10^{-3}$ and $\lambda = 1$. The critical Weber number for splashing, We^*, is calculated as the minimum value of We for which the curves cross the horizontal line $C_b = We^{1/2}\sqrt{b/8}\,db/dt = 0.1 \pm 0.005$. Notice that We^* increases with Oh and λ namely, as the shear stress with the substrate increases.

and which reduces to:

$$t_e \simeq 1.05 We^{-2/3} \tag{9}$$

in the limit $Oh \to 0$ [14].

Using the expression of t_e given by either Eq. (8) or by Eq. (9), the ordinary differential equations in (3) are then solved subjected to the following initial conditions, deduced making use of potential flow theory [14, 34]:

$$s(t_e) = \sqrt{3t_e}\,, \quad b(t_e) = \frac{\sqrt{12}}{\pi} t_e^{3/2} \quad \text{and} \quad v(t_e) = \frac{1}{2}\sqrt{\frac{3}{t_e}}\,. \tag{10}$$

The system of equations (3)-(4) subjected to the initial conditions given in (10) with t_e calculated using Eq. (8) is solved for two values of the friction factor, $\lambda = 0$ and $\lambda = 1$, for different values of We and Oh -notice that $Re = \sqrt{We}Oh^{-1}$, and the value of $We^{1/2}\sqrt{b/8}\,db/dt$, which should be such that $We^{1/2}\sqrt{b/8}\,db/dt < 0.1$ for the rim to break into drops as a consequence of the growth of capillary disturbances, see Eq. (2), is represented as a function of time in Fig. 8. The results in Fig. 8 reveal that the value of the critical Weber number for splashing, We^*, namely, the minimum value of We for which $We^{1/2}\sqrt{b/8}\,db/dt < 0.1$, decreases as the wall shear stress decreases: indeed, notice that larger values of λ or Oh yields to larger values of We^*, a fact indicating that the splash transition is

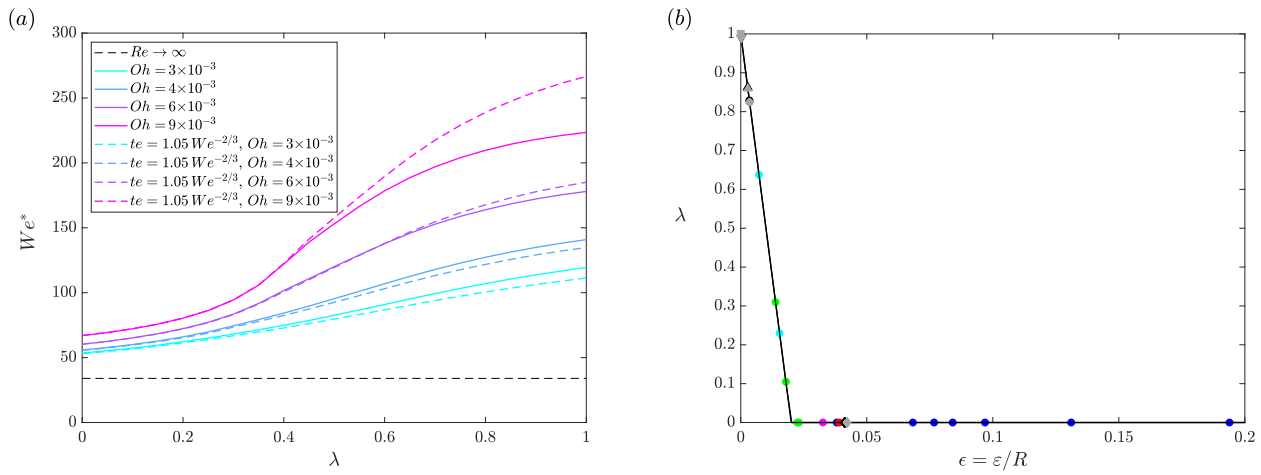

FIG. 9. (a) The values of We^* calculated following the procedure illustrated in Fig. 8 using either Eq. (8) (continuous lines) or the approximate value in the low-Oh limit in [14] $t_e = 1.05\,We^{-2/3}$ (dashed lines), are represented as a function of λ for four different values of Oh. The value of We^* corresponding to the potential flow case, $Re \to \infty$, is indicated with a horizontal black dashed line. The results in this figure clearly show that We^* increases with Oh and λ namely, as the shear stress with the substrate increases. (b) The friction factor λ is calculated as a function of the values of ϵ given in tables III and IV by means of Eq. (7) using $\epsilon_0 = 0.02$ (black continuous line).

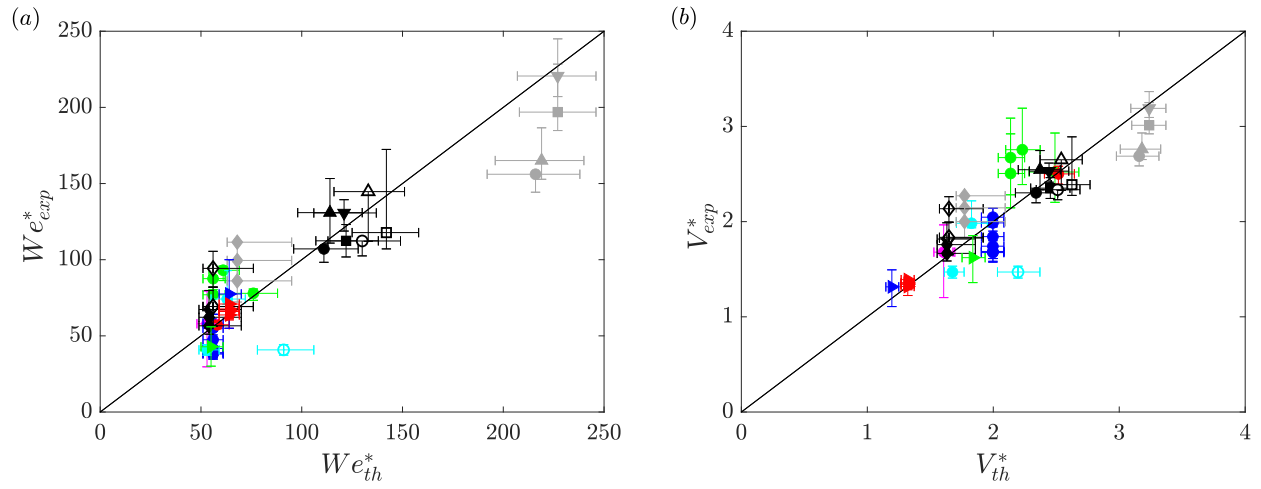

FIG. 10. Comparison between the experimental values of (a) the critical Weber number and (b) the critical velocity for splashing given or deduced from tables III and IV and the corresponding values calculated solving the system of Eq. (3)-(4) complemented with Eq. (7) for $\lambda(\epsilon)$ using $\epsilon_0 = 0.02$, see also Figs. 8-9. Notice that $\lambda = 0$ for the case of drops impacting in the Leidenfrost regime and also for the superhydrophobic substrates created by depositing one (SH2), two (SH1) or three (SH0) layers of Neverwet over a glass substrate, see tables II-III.

delayed if the fluxes of mass and momentum into the rim are reduced, see Eq. (3). Now, the system (3), subjected to the initial conditions (10) calculated using the value of the ejection time t_e given by either (8) or by (9) is solved for different values of We and Oh for λ varying continuously from $\lambda = 0$ to $\lambda = 1$ and the values of the critical Weber number obtained are represented as a function of λ in Fig. 9a. As expected, the values of We^* calculated using either Eq. 8 or Eq. 9 are very close to each other except for the largest value of Oh considered here, $Oh \approx 0.01$ and, even in this case, the differences are only appreciable when $\lambda \approx 1$. Nevertheless, here we have made use of the equation for the ejection time given in Eq. (8) since this expression retains the effect of the liquid boundary layer and, then, of the liquid viscosity, which is varied in our experimental study. Finally, in order to compare our predictions with the experimental measurements provided in Fig. 6, also given in tables III and IV, Eqs. (3) need to be solved using equation (7), which depends on just one free parameter, ϵ_0. We have found that an optimum agreement between experiments and predictions can be achieved for $\epsilon_0 = 0.02$. Figure 9b reveals that, since the

superhydrophobic substrates created by superimposing different layers of Neverwet possess a value of the roughness that can vary within the range $\varepsilon = 60 \pm 40$ μm [3, 20], the value of their relative roughness is $\epsilon \geq 0.02$. Consequently, in these cases, the value of the friction factor is the same as for the case of drops impacting a superheated substrate in the dynamic Leidenfrost regime, $\lambda = 0$ and, therefore, the value of the friction factor in these cases is insensitive to the precise value of ε.

The experimental values of the critical Weber number and of the corresponding critical velocity for splashing given in tables III and IV for drops of different radii and viscosities impacting over different types of superhydrophobic substrates or in the Leidenfrost regime, are compared in Fig. 10 with the solution of Eqs. (2)-(4) and (7) using $\epsilon_0 = 0.02$. The results in Fig. 10 show a good agreement between experiments and predictions, thus validating our approach and confirming our initial hypothesis that the splash velocity decreases for smaller values of the wall shear stress. Indeed, notice that Eq. (7) indirectly expresses that the friction factor, which is $\lambda = 0$ for the case of Leidenfrost drops, decreases with the amount of air entrapped between the superhydrophobic substrate and the wall. This is so because the air entrapped in the corrugations increases with ϵ, as it is clearly shown in the experiments depicted in Figs. 2 and 5. Let us finally point out here that the results in Fig. 10 corresponding to drops impacting in the Leidenfrost regime also reproduce the value of the critical Weber number for splashing reported in [28].

CONCLUSIONS

In this contribution we have analyzed the influence of the liquid viscosity and of the substrate roughness on the splash transition of drops impacting different types of superhydrophobic substrates. Our experimental results reveal that larger values of the wall shear stresses contribute to delay the splash transition. We have also provided an empirical equation with just one adjustable parameter relating the friction factor λ in the theory by [34] with the relative roughness ϵ, which indirectly expresses that λ decreases when the amount of air entrapped at the substrate corrugations increases. In fact, the proposed equation for $\lambda(\epsilon)$ also states that $\lambda = 0$ when the amount of air entrapped is above a certain threshold. The values of the critical Weber number for the transition to splashing, $We^*(\epsilon, Oh)$, calculated using the models in [1, 34] complemented with the empirical equation for $\lambda(\epsilon)$ proposed here, compare favourably with experiments performed using different types of superhydrophobic substrates, different drop radii and different liquids and also reproduce the results in [28] for the case of drops impacting in the Leidenfrost regime.

APPENDIX

It could be thought that the dependence of the critical Weber number for splashing with the type of superhydrophobic substrate is caused by the different values of the dynamic advancing contact angles. This possibility is explored in Fig. 11, where the critical Weber number calculated solving Eqs. (3)-(4), (8), (10) once the term $-2We^{-1}$ in Eq. (3) is replaced by $-(1-\cos\theta_d)\,We^{-1}$, is represented as a function of θ_d for $\lambda = 1$ and four values of Oh. The predictions in figure 11 indicate that the critical Weber number should decrease when the value of the dynamic advancing contact angle decreases. However, this result contrasts with the trends observed in tables II and III, where the superhydrophobic substrates SH0 and SH1, which possess the larger values of the advancing contact angle, are associated with the smaller values of the critical Weber numbers. Hence, the result in Fig. 11 support our main conclusion that, for the case of superhydrophobic substrates, the measured larger values of the critical splash velocity are mainly caused by larger values of the shear stress at the wall.

ACKNOWLEDGMENTS

This work has been supported by the Grant PID2020-115655G, financed by the Spanish MCIN/ AEI/10.13039/501100011033.

* Email address for correspondence: jgordill@us.es

[1] E. S. Quintero, G. Riboux, and J. M. Gordillo, Splashing of droplets impacting superhydrophobic substrates, Journal of Fluid Mechanics **870**, 175 (2019).

[2] J. Bird, R. Dhiman, H.-M. Kwon, and K. Varanasi, Reducing the contact time of a bouncing drop, Nature **503**, 385 (2013).

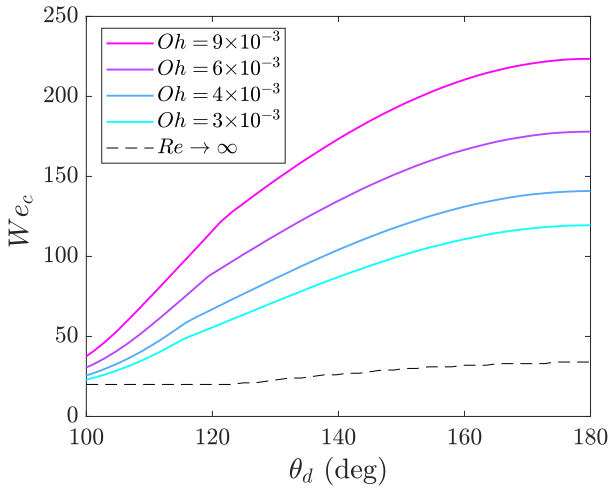

FIG. 11. Values of the critical Weber numbers as a function of the advancing contact angle θ_d obtained solving Eqs. (3)-(4), (8), (10) for the case in which the term $-2We^{-1}$ in Eq. (3) is replaced by $-(1-\cos\theta_d)\,We^{-1}$ with $\lambda = 1$ and different values of Oh.

[3] S. Kim, Z. Wu, E. Esmaili, J. J. Dombroskie, and S. Jung, How a raindrop gets shattered on biological surfaces, Proceedings of the National Academy of Sciences of the United States of America **117**, 13901 (2020).
[4] W. Barthlott and C. Neinhuis, Purity of the sacred lotus, or escape from contamination in biological surfaces, Planta **202**, 1 (1997).
[5] S. Shibuichi, T. Onda, N. Satoh, and K. Tsujii, Super water-repellent surfaces resulting from fractal structure, Journal of Physical Chemistry **100**, 19512 (1996).
[6] J. Bico, C. Marzolin, and D. Quéré, Pearl drops, Europhysics Letters (EPL) **47**, 220 (1999).
[7] R. Blossey, Self-cleaning surfaces virtual realities, Nature Materials **2**, 301 (2003).
[8] D. Quéré, Non-sticking drops, Reports on Progress in Physics **68**, 2495 (2005).
[9] M. Callies and D. Quéré, On water repellency, Soft Matter **1**, 55 (2005).
[10] D. Qur, Wetting and roughness, Annual Review of Materials Research **38**, 71 (2008).
[11] J. Wang, H. Chen, T. Sui, A. Li, and D. Chen, Investigation on hydrophobicity of lotus leaf: Experiment and theory, Plant Science **176**, 687 (2009).
[12] M. A. Quetzeri-Santiago, A. A. Castrejón-Pita, and J. R. Castrejón-Pita, The effect of surface roughness on the contact line and splashing dynamics of impacting droplets, Scientific Reports **9**, 1 (2019).
[13] M. A. Quetzeri-Santiago, K. Yokoi, A. A. Castrejón-Pita, and J. R. Castrejón-Pita, Role of the dynamic contact angle on splashing, Phys. Rev. Lett. **122**, 228001 (2019).
[14] G. Riboux and J. M. Gordillo, Experiments of drops impacting a smooth solid surface: A model of the critical impact speed for drop splashing, Phys. Rev. Lett. **113**, 024507 (2014).
[15] P. Garca-Geijo, E. S. Quintero, G. Riboux, and J. M. Gordillo, Spreading and splashing of drops impacting rough substrates, Journal of Fluid Mechanics **917**, A50 (2021).
[16] C. D. Stow, M. G. Hadfield, and J. M. Ziman, An experimental investigation of fluid flow resulting from the impact of a water drop with an unyielding dry surface, Proc. R. Soc. Lond. **373**, 419441 (1981).
[17] C. Mundo, M. Sommerfeld, and C. Tropea, Droplet-wall collisions: Experimental studies of the deformation and breakup process, Int. J. Multiphase Flow **21**, 151 (1995).
[18] K. Range and F. Feuillebois, Influence of surface roughness on liquid drop impact., J. Colloid Interf. Sci. **203**, 16 (1998).
[19] L. Chen, Z. Xiao, P. C. Chan, Y.-K. Lee, and Z. Li, A comparative study of droplet impact dynamics on a dual-scaled superhydrophobic surface and lotus leaf, Applied Surface Science **257**, 8857 (2011).
[20] R. Gupta, V. Vaikuntanathan, and D. Sivakumar, Superhydrophobic qualities of an aluminum surface coated with hydrophobic solution neverwet, Colloids and Surfaces A: Physicochemical and Engineering Aspects **500**, 45 (2016).
[21] J. Hao, Effect of surface roughness on droplet splashing, Physics of Fluids **29**, 122105 (2017).
[22] C. Tang, M. Qin, X. Weng, X. Zhang, P. Zhang, J. Li, and Z. Huang, Dynamics of droplet impact on solid surface with different roughness, International Journal of Multiphase Flow **96**, 56 (2017).
[23] T. de Goede, K. de Bruin, N. Shahidzadeh, and D. Bonn, Droplet splashing on rough surfaces, Phys. Rev. Fluids **6**, 043604 (2021).
[24] H. Kim, C. Lee, M. H. Kim, and J. Kim, Drop impact characteristics and structure effects of hydrophobic surfaces with micro- and/or nanoscaled structures, Langmuir **28**, 11250 (2012).
[25] H. Kim, U. Park, C. Lee, H. Kim, M. Hwan Kim, and J. Kim, Drop splashing on a rough surface: How surface morphology affects splashing threshold, Applied Physics Letters **104**, 161608 (2014).

[26] D. G. K. Aboud and A.-M. Kietzig, Splashing threshold of oblique droplet impacts on surfaces of various wettability, Langmuir **31**, 10100 (2015).
[27] T. Tran, H. J. J. Staat, A. Prosperetti, C. Sun, and D. Lohse, Drop impact on superheated surfaces, Phys. Rev. Lett. **108**, 036101 (2012).
[28] G. Riboux and J. M. Gordillo, Maximum drop radius and critical weber number for splashing in the dynamical leidenfrost regime, J. Fluid Mech. **803**, 516 (2016).
[29] Y. Wang, A. El Bouhali, S. Lyu, L. Yu, Y. Hao, Z. Zuo, S. Liu, and C. Sun, Leidenfrost drop impact on inclined superheated substrates, Physics of Fluids **32**, 112113 (2020).
[30] R. Saggin and J. N. Coupland, Rheology of xanthan/sucrose mixtures at ultrasonic frequencies, Journal of Food Engineering **65**, 49 (2004).
[31] C. A. E. Hamlett, S. Atherton, N. J. Shirtcliffe, G. McHale, S. Ahn, S. H. Doerr, R. Bryant, and M. I. Newton, Transitions of water-drop impact behaviour on hydrophobic and hydrophilic particles, European Journal of Soil Science **64**, 324 (2013).
[32] H. J. J. Staat, T. Tran, B. Geerdink, G. Riboux, C. Sun, J. M. Gordillo, and D. Lohse, Phase diagram for droplet impact on superheated surfaces, J. Fluid Mech. **779**, R3 (2015).
[33] L. Liu, G. Cai, and P. A. Tsai, Drop impact on heated nanostructures, Langmuir **36**, 10051 (2020).
[34] J. M. Gordillo, G. Riboux, and E. S. Quintero, A theory on the spreading of impacting droplets, Journal of Fluid Mechanics **866**, 298 (2019).
[35] G. Riboux and J. M. Gordillo, The diameters and velocities of the droplets ejected after splashing, J. Fluid Mech. **772**, 630 (2015).
[36] W. S. Rayleigh, On the instability of jets, Proc. of the London Math. Soc. **10**, 4 (1878).
[37] J. Eggers and E. Villermaux, Physics of liquid jets, Rep. Prog. Phys. **71**, 036601 (2008).
[38] S. Wildeman, C. W. Visser, C. Sun, and D. Lohse, On the spreading of impacting drops, J. Fluid Mech. **805**, 636 (2016).
[39] I. V. Roisman, Inertia dominated drop collisions. ii. an analytical solution of the navier-stokes equations for a spreading viscous film, Phys. Fluids **21**, 052104 (2009).
[40] P. Chantelot and D. Lohse, Drop impact on superheated surfaces: short-time dynamics and transition to contact, Journal of Fluid Mechanics **928**, A36 (2021).